A Nonlinear Extended State Observer for Rotor Position and Speed Estimation for Sensorless IPMSM Drives

Zhuang Xu, *Member, IEEE*, Tianru Zhang, Yuli Bao, He Zhang and Chris. Gerada, *Senior Member, IEEE*

***Abstract*- Sensorless machine drives in vehicle traction frequently experience rapidly-changing load disturbance and demand fast speed dynamics. Without gain-scheduling or compensation, conventional Quadrature Phase-Locked-Loop (Q-PLL) is unable to accurately estimate the rotor position and speed for these systems. In this paper, a Third-Order Nonlinear Extended State Observer (TNESO) is proposed for position and speed estimation for sensorless Interior Permanent Magnet Synchronous Motor (IPMSM) drives. TNESO has the power of nonlinear feedback and takes the advantages of fast convergence and disturbance rejection. An optimized parameter configuration method is deployed to extend the disturbance observation bandwidth of the TNESO. Both steady state and transient performance of TNESO are verified through the experimental tests. In comparison with the performance of conventional Q-PLL scheme, the proposed observer is proved to be capable of delivering higher precision of position and speed estimation against rapidly varying disturbance in wide operating range.**

I. INTRODUCTION

Permanent Magnet Synchronous Motors (PMSMs) are widely used in the applications where require high precision and high dynamic performance. In vehicle traction, the mechanical sensor, which is a weak link in drive systems, can be eliminated in sensorless operations since such sensor brings disadvantages and limitations in terms of cost and reliability. IPMSMs have been commercialized as the main traction motors for hybrid electric vehicles (HEVs) and electric vehicles (EVs). Although numerous sensorless techniques [1-6] have been developed for automotive applications, due to the restrict requirements of extremely high safety, the rotor position sensor cannot be replaced entirely.

The overview of the techniques of sensorless control can be classified into two main categories based on operating principles: fundamental-model based methods [4-11] and signal injection techniques [12-14] depending on rotor anisotropy. The first category consists of the methods of using either EMF estimation or estimated stator flux linkage. At present, there are mainly five closed-loop observer techniques: Extended Kalman Filters (EKF) [8], Model Reference Adaptive Systems (MRAS) [9], Sliding Mode Observers (SMO) [10, 16], Extended State Observers (ESO) [17-22] and Adaptive Filters [23-24]. However, the fundamental-frequency observers reach their limits at zero stator frequency where the back emf gets to zero and the IPMSM is rendered unobservable. The methods in the second category [12-14] deals with the situation where fundamental-model methods lose performance. Anisotropic properties can be exploited to retrieve rotor position information. Either voltage or current signals at the frequencies other than the fundamental ones can be injected to transiently excite IPMSM and detect the spatial orientations of existing anisotropies. Nevertheless, high-frequency signal injection results in undesirable torque ripples, vibrations and acoustic noises. Apart from closed-loop sensorless schemes, open-loop methods that do not need sensorless observers such as V/f or I/f [25] have been proposed. But they might not be able to deal with the controlled drive system that requires high-quality transient profile.

In relatively low, medium or high speed region, sensorless control using fundamental-frequency signals has been widely consolidated. Regardless of what signal is chosen, it is essential to estimate the rotor position and speed at the last stage in sensorless operation. A direct approach [6-8] to the position estimation of IPMSM rotor utilizes the inverse trigonometric function based on estimated back-EMF space vector. However, the estimation quality highly relies on the waveforms of the back-EMF that may be distorted by inverter nonlinearity, parameter detuning and measurement offsets. The distortion will result in deviation of the phase and frequency. A common technique to solve this problem is to track the phase and frequency of the estimated back-EMF by means of Q-PLL [15-16].

Normally, the structure of Q-PLL contains a linear PI regulator as error correction mechanism. The regulator can be easily configured and tuned to minimize input error. Nevertheless, there are four fundamental drawbacks [17] to be addressed: 1) unexpected overshoots; 2) limited control capability; 3) Inefficiency of the linear weighted sum of the P and I terms; 4) Less capability of dealing with time-varying perturbation. Although phase compensators can be adopted to adjust the control bandwidth and phase margin. However, Q-PLL bandwidth varies as the speed and load torque changes if the speed-dependent loop gains are kept constant.

To overcome the drawbacks of conventional Q-PLL, state observers [6] were introduced in cascade with EMF observer to

Supported by the Ningbo Science & Technology Bureau under Grant 2014A35007 and Zhejiang Provincial Natural Science Foundation of China under Grant No. LGG19E070009. Zhuang Xu john.xu@nottingham.edu.cn
Tianru Zhang tianru.zhang@nottingham.edu.cn Yuli Bao Yuli.Bao@nottingham.edu.cn He Zhang he.zhang@nottingham.edu.cn Chris.Gerada chris.gerada@nottingham.ac.uk

This article has been accepted for publication in a future issue of this journal, but has not been fully edited. Content may change prior to final publication. Citation information: DOI 10.1109/TPEL.2019.2914119, IEEE Transactions on Power Electronics

enhance the estimation accuracy and transient performance. Among them, ESO is a competitive candidate. Original Nonlinear ESO (NESO) was developed by Han [17], along with the theory on the active disturbance rejection control (ADRC). Later, Gao [18] linearized and parameterized the nonlinear form. Linear ESO (LESO) is superior to NESO in parameter tuning and theoretical analysis. Gao also proposed optimal observer bandwidth for fast tracking of disturbance and uncertainty. However, the observation efficiency of NESO is higher than that of LESO [19]. The control performance of NESO is obvious but the parameter tuning method is very different from the counterpart linear observer [19].

This paper proposes a Third Order NESO (TNESO) with a non-linear feedback structure. This enables rapid convergence and very fast dynamic response. One of the current issues with ESOs is that the task of adjusting parameters is more complicated. There are two key points with regards to good observation performance [17-18]. Firstly, it is necessary to ensure operation stability. Secondly, it is essential to guarantee the tracking performance and the accuracy of the disturbance observation. The stability analysis for high order ESO is more difficult due to its strong nonlinearity. This paper presents the stability analysis for the proposed TNESO. At present, there are few researches exploiting on ESO parameter tuning. The paper [17] reveals the close relationship between ESO parameter selection and famous Fibonacci sequence through a large number of simulations. Nevertheless, the relationship between parameter tuning and the disturbance observation performance has not been analyzed theoretically. For NESO [19], it is proposed that the parameters can be dynamically determined by setting the poles of compensation matrix. But this method is only suitable for the ESO with smooth differentiable nonlinear functions and cannot be applied to the ESO having non-smooth function. In addition, there are some parameter optimization methods using genetic algorithm and Lyapunov function method. But quite a lot of simulation calculations are needed. Some are only applicable to the second order. In general, the relationship between performance index and parameters of disturbance observation needs to be further investigated. The current issues to be solved are how to analyze control performance, find out the relationship between parameters and performance and put forward the optimization method.

II. Conventional Extraction of the Position and Speed by PLLs

The conventional system structure for estimating position and speed is illustrated in Fig. 1. The front-end observer [2-8] estimates the Extended EMF (EEMF) based on the fundamental-model of IPMSMs. The diverse structures it takes can be summarized into the extended Kalman filter, model reference adaptive system, variable structure and adaptive observers. If the estimated EEMF is extracted from high switching signals or contains high frequency noises or dc components, some types of filtering may be required to remove those additional signals.

The estimated EEMF $\hat{E}_{\alpha\beta}$ have position information. The extensively-adopted technique is to trace the phase and

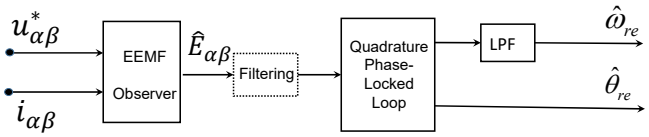

Fig. 1. The overall structure of conventional Position and speed estimation.

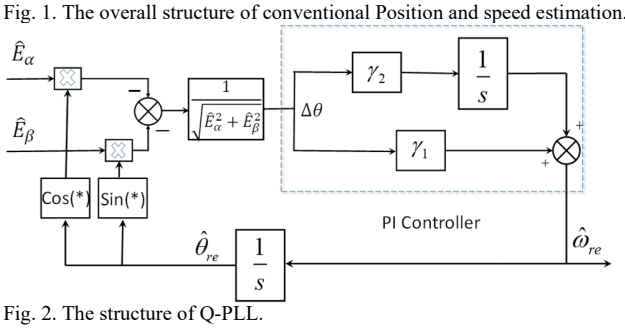

Fig. 2. The structure of Q-PLL.

frequency by means of PLLs. The fundamental operation of Q-PLL [15,16] is to obtain the phase error of the input and output signals by phase detector. The error signal $\Delta\theta$ of the rotor position can be constructed by heterodyne method from $\hat{E}_{\alpha\beta}$ and the estimated rotor angle $\hat{\theta}_{re}$ in (1) and (2).

$$\varepsilon(\Delta\theta) = -\hat{E}_\alpha \cos\hat{\theta}_{re} - \hat{E}_\beta \sin\hat{\theta}_{re} = \sqrt{\hat{E}_\alpha{}^2 + \hat{E}_\beta{}^2}\sin(\theta_{re} - \hat{\theta}_{re}) \quad (1)$$

When the tracking error gets sufficiently smaller, the displacement can be expressed as:

$$\Delta\theta \approx \sin(\theta_{re} - \hat{\theta}_{re}) = \frac{\varepsilon(\Delta\theta)}{\sqrt{\hat{E}_\alpha{}^2 + \hat{E}_\beta{}^2}} \quad (2)$$

Based on the operating principal, a Q-PLL for the rotor speed and position estimation is sketched in Fig. 2.

The basic operating principle of PI-based PLL follows error-based feedback control with little or no knowledge about the plant dynamics. Although the gains can be configured and tuned to fulfil tasks, due to the fundamental limitations, the PI controller is unable to deal with the controlled system that requires high-quality transient profile. It is still challenging to find a time-optimal solution that guarantees the fastest convergence without any overshoot. The linear combination of the present and accumulative forms of the tracking error has less capability of reducing steady state error significantly [17].

The most difficult part of the PLL design is that the drive system frequently experiences external load disturbance and demands fast-changing speed profile. To achieve a fast extraction of the position and speed in wide operating range, the input to the Q-PLL can be normalized first before it goes directly to phase locking stage. This can be implemented by taking the EEMF vector magnitude as scaling factor. A modified scheme is illustrated in Fig. 3. The advantage of this improvement is that the fundamental component can be preserved while high order harmonics will be eliminated to reduce noise propagation.

To further increase the estimation bandwidth, a linear extended Luenberger observer has been proposed [26]. As shown in Fig. 4, the bandwidth can be expanded by inserting a torque feedforward term into PLL structure. The estimated

This article has been accepted for publication in a future issue of this journal, but has not been fully edited. Content may change prior to final publication. Citation information: DOI 10.1109/TPEL.2019.2914119, IEEE Transactions on Power Electronics

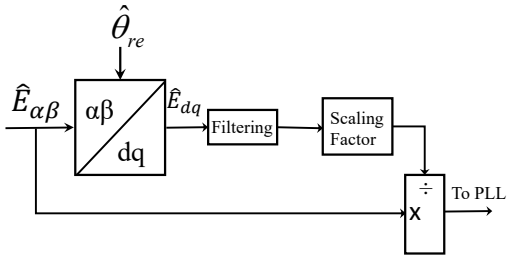

Fig. 3. EEMF normalization for constant bandwidth PLL.

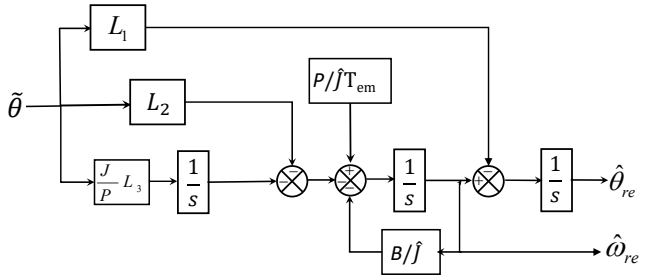

Fig. 4. Position and speed estimations by a linear ESO Luenberger estimator [27].

speed was modified to be the output of an integrator that filters the noises on the theta error given by the emf estimation. In [27], the position and speed errors were extracted by splitting the actual speed into the estimated and error terms. In addition, the position and speed estimator attempted to nullify the speed error in the steady state. However, the estimator still resulted in unexpected steady-state speed error in certain speed region. Moreover, the gain setting lacks analytical guidance and becomes more difficult since the position estimation error is influenced by parameter detuning and external disturbances. The disadvantages discussed above provoke more advanced scheme that is expected to provide high precision and robustness of the estimations.

III. Proposed 3rd order ESO for Position and Speed Estimation

To acquire more accurate position and speed estimation under fast loading conditions, Q- PLL schemes can be replaced by removing the PI regulator and eliminating the linear gains. The method to be considered is a nonlinear form of extended state observer. The construction of the observer is demonstrated as follows.

The mechanical equation of the IPMSMs with machine parameter uncertainties is expressed as:

$$\dot{\omega}_r = (a+\Delta a)i_q + (b+\Delta b)i_d i_q - (c+\Delta c)\omega_r - (d+\Delta d)T_L \quad (3)$$

where $a=1.5P_n\lambda_f/J$; $b=1.5P_n(L_d-L_q)/J$; $c=B/J$; $d=1/J$. P_n is the number of pole pairs. B is the friction coefficient and J is the moment of inertia of the machine. i_d and i_q are the currents on d-q axis. T_L is the load torque. Δa, Δb, Δc and Δd represent perturbation values due to the parameter variations. Let $g = a\cdot(i_q - i_q^*) + \Delta a\cdot i_q + (b+\Delta b)i_d i_q - (c+\Delta c)\omega_r - (d+\Delta d)T_L$. i_q^* is the reference for q-axis current. Equation (3) can be rearranged to be $\dot{\omega}_r = a\cdot i_q^* + g$. g represents uncertainties and can be considered to be the disturbance to the speed dynamics. In the case that the unknown disturbance varies suddenly and machine parameters detune, the disturbance magnitude also increases. Thanks to the strong estimation capability of the 3rd order ESO, g can be observed and compensated. g is defined to be an extended state and $\dot{g} = w(t)$. The mechanical dynamics of the anisotropic PMSM are extended to be:

$$\begin{cases} \dot{\theta} = \omega_r \\ \dot{\omega}_r = a\cdot i_q^* + g \\ \dot{g} = w(t) \end{cases} \quad (4)$$

A nonlinear feedback function [19] in (5) is used to establish a non-smooth feedback to enhance the capability of rejecting disturbances and estimating uncertainties.

$$fal(\varepsilon) = \begin{cases} \dfrac{\varepsilon}{\delta^{1-\alpha}} & |\varepsilon| \le \delta \\ |\varepsilon|^{\alpha}\,\mathrm{sgn}(\varepsilon) & |\varepsilon| > \delta \end{cases} \quad (5)$$

Power α and linear range δ are important parameters to be predetermined. An effective value can be assigned to α[17]. Therefore, the extended state observer (Fig. 5) takes the following form:

$$\begin{cases} e_1 = \hat{\theta} - \theta \\ \dot{\hat{\theta}} = \hat{\omega}_r - \beta_1 e_1 \\ \dot{\hat{\omega}}_r = z + a\cdot i_q^* - \beta_2\cdot fal(e_1) \\ \dot{z} = -\beta_3\cdot fal(e_1) \end{cases} \quad (6)$$

where e_1 is the displacement between the estimated and actual rotor position. β_1, β_2 and β_3 are positive parameters to be determined. z tracks g. The linear range δ is further considered. Define $F = fal(e_1)/e_1$. Then $fal(e_1) = Fe_1$. Thus, *fal* can be seen as a linear function e_1 with varying gain. To make the system states recover quickly during the transient period and reduce the effect of the measurement noise afterward, the steady-state error should be located in the nonlinear range of the function F, i.e. $\delta < e_1$. ESO has fast state reconstruction and good measurement noise attenuation. Therefore, due to the simple nonlinear function, NESO has the merits of the improved high-gain observers [17,19].

Defining $e_2 = \hat{\omega}_r - \omega_r$ and $e_3 = z - g$ and subtracting (4) from (6) yield a 3rd order error dynamics:

$$\begin{cases} \dot{e}_1 = e_2 - \beta_1 e_1 \\ \dot{e}_2 = e_3 - \beta_2\cdot fal(e_1) \\ \dot{e}_3 = -\beta_3\cdot fal(e_1) - w(t) \end{cases} \quad (7)$$

The problem formulation is that for the bounded and uncertain function *w(t)*, how to set *fal* function's coefficients, gains β_1, $\beta_2$and β_3 to force the errors e_1, e_2 and e_3 to converge as small as possible at a fast rate.

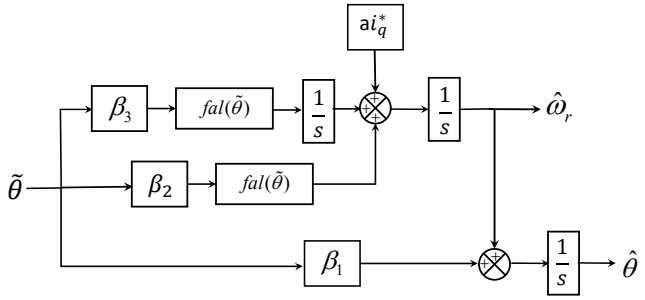

Fig. 5. Position and speed extraction by TNESO.

It is seen that the error signal of the rotor position is constructed by the heterodyne method from the estimated EEMF and the angle produced by (1) and (2). Therefore, TNESO does the retrieval of the rotor position and speed at the last stage. The estimation process does not rely on anisotropic rotor structure. This method can be generalized for both IPMSMs and Surface Mounted Permanent Magnet synchronous motors (SPMSM).

A. Stability Analysis of ESO Error Dynamics

It can be proven below by means of Lyapunov's direct method that the error system (7) is asymptotically stable at the equilibrium point. The state equation can be expressed as:

$$\dot{e} = -A(e)\cdot e \tag{8}$$

where $e = \left[e_1, e_2, e_3\right]^T$

$$A(e) = \begin{bmatrix} \beta_1 & -1 & 0 \\ \beta_2 F & 0 & -1 \\ \beta_3 F & 0 & 0 \end{bmatrix} \tag{9}$$

In (9), apparently $F > 0$ and has a boundary. If the following condition can be satisfied,

$$\beta_1\beta_2 F - \beta_3 F > 0 \tag{10}$$

Then a matrix D with positive main diagonal elements can be designated:

$$D = \begin{bmatrix} 1 & h(e_1)+\delta_1 & -\gamma \\ -h(e_1)-\delta_1 & \gamma & g(e_1)+\delta_2 \\ \gamma & -g(e_1)-\delta_2 & \gamma \end{bmatrix} \tag{11}$$

where γ, δ_1 and δ_2 are all positive infinitesimal. $DA(e)$ can be enabled to be positive definite symmetric matrices with:

$$h(e_1) = \frac{\beta_2 F}{\beta_1\beta_2 F - \beta_3 F};\ g(e_1) = \frac{1}{\beta_1\beta_2 F - \beta_3 F} \tag{12}$$

Let

$$V = \int_0^t (DA(e)e,\dot{e})d\tau + C = -\int_0^t \{-(\beta_1 e_1 - e_2)^2 - \gamma[\beta_2 fal(e_1) - e_3]^2 - \gamma[\beta_3 fal(e_1) + w(t)]^2\}d\tau + C \tag{13}$$

be a Lyapunov function candidate. C is chosen to be sufficiently large positive constant. $V > 0$ is guaranteed. Therefore V is a Lyapunov function. The derivative of V is calculated as:

$$\dot{V} = -(\beta_1 e_1 - e_2)^2 - \gamma[\beta_2 fal(e_1) - e_3]^2 - \gamma[\beta_3 fal(e_1) + w(t)]^2 \le 0 \tag{14}$$

By Lyapunov stability theorem, only if (7) has zero solutions, the system are asymptotically stable at the equilibrium point. As $F > 0$, (10) leads to $\beta_1\beta_2 - \beta_3 > 0$. Only if ESO (6) satisfies this condition, it can be proven that the error system (7) are asymptotically stable.

B. Analysis of Disturbance Observation Capability and Parameter Optimization.

1) Capability of observing disturbance

To analyze the capability of the ESO's disturbance observation, by applying Laplace transformation to (6) , the state space equations in continuous-time is written as below:

$$\begin{cases} \hat{\theta}s = \hat{\omega}_r - \beta_1 e_1 \\ \hat{\omega}_r s = z + a\cdot i_q^* - \beta_2 F e_1 \\ zs = -\beta_3 F e_1 \end{cases} \tag{15}$$

The transfer function between the extended state z and the estimated state $\hat{\theta}$ together with control input i_q^* can be derived.

$$z = \frac{\beta_3 F}{s^3 + \beta_1 s^2 + \beta_2 F s + \beta_3 F} f = G_f(s) f \tag{16}$$

where $f = \theta s^2 - a i_q^*$ is the total disturbance to be observed by the ESO. The input ai_q^* is known. From (16), the observation performance for f through z entirely depends on the characteristics of $G_f(s)$. To achieve better estimation accuracy, the gain response is expected to be $\left|G_f(s)\right| = 1$ within the disturbance bandwidth. Assuming the active band of f is [0, ω_c] in which $\left|G_f(s)\right| = 1$, i.e. $z = -\beta_3 F f$. At this stage, the key to the ESO design for the purpose of better immunity to disturbance is how to configure the parameters β_1, β_2 and β_3 such that $\left|G_f(s)\right|$ always approximates to 1 in the specific frequency band. A natural thought is to extend $G_f(s)$ bandwidth by assigning optimal poles based on the analysis of the influence on poles due to F variation.

2) Optimal gain selection considering the influence of F variation

Apparently, the operating point of the nonlinear *fal* function varies against e_1. The variation of F leads to the change of $G_f(s)$'s pole location and affects the observation bandwidth of disturbance. According to the pole placement method for linear ESOs [18], three poles are configured to the same value ρ at certain operating point.

$$s^3 + \beta_1 s^2 + \beta_2 F s + \beta_3 F = (s+\rho)^3 \tag{17}$$

If e_1 gets close to zero, then $F=1$. Accordingly, $\beta_1 = 3\rho$, $\beta_2 = 3\rho^2$ and $\beta_3 = \rho^3$. Nevertheless, F is a function of the *fal* function and e_1 and will cause the poles' position to move. Substituting the calculated gains into (17) gives

$$s^3 + 3\rho s^2 + 3\rho^2 F s + \rho^3 F = 0 \tag{18}$$

The solutions to (18) can be resolved. The characteristics equation (18) has one real root s_1 and two complex roots s_2 and s_3. The system bandwidth is determined by the root that sits nearest to the imaginary axis. So the observation bandwidth of the ESO can be represented by the following formula.

This article has been accepted for publication in a future issue of this journal, but has not been fully edited. Content may change prior to final publication. Citation information: DOI 10.1109/TPEL.2019.2914119, IEEE Transactions on Power Electronics

$$r_d = \min(|r_1|, |r_2|) \tag{19}$$

where

$$r_1 = s_1 = -\rho\left[1 + \sqrt[3]{1-F}\left(\sqrt[3]{1+\sqrt{F}} + \sqrt[3]{1-\sqrt{F}}\right)\right] \tag{20}$$

$$r_2 = real(s_{2,3}) = -\rho\left[1 - 0.5\cdot\sqrt[3]{1-F}\left(\sqrt[3]{1+\sqrt{F}} + \sqrt[3]{1-\sqrt{F}}\right)\right] \tag{21}$$

Based on the analysis and derivation, it can be found that the change of F affects the roots of the characteristic equation. If the poles assignment follows (17), the real parts of the roots s_1, s_2 and s_3 will vary with F value. r_2 has the minimum value of $-\rho$ when F equals 1 at which r_1 reaches its peak value at -ρ. Therefore, $r = |r_2|$. The real part of the complex roots is closer to the imaginary axis.

Set $\rho = 1000$, the real parts of the three roots of (18) will move as F changes. The trajectories are plotted in Fig. 6 against the F value. It can be seen that only if $F=1$, the real parts are equal and reach the peak of $r_d = \rho$. Elsewhere $r_d < \rho$. This indicates that wherever the poles are placed, the change of F will cause the observer bandwidth to decrease.

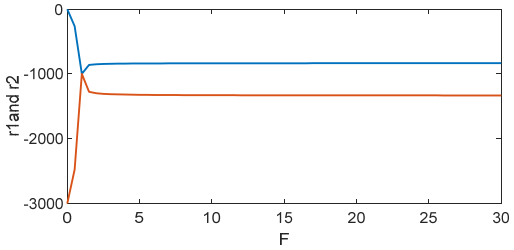

Fig. 6. r_1 and r_2 against F variation.

Under the most operating conditions, $F \neq 1$. There will be a maximum distance from the root representing the observer bandwidth to the imaginary axis. Assuming that the maximum bandwidth appears at $F = F_0$, F can be defined as $F = \frac{F'}{F_0}$. The variation of F' is equivalent to that of F. The conclusion is that if the poles are placed at F_0 or other values, the ESO bandwidth will change with respect to F'. If $F' > F_0$, when $F \to \infty$, $r_d = r_2$. The bandwidth will be lower than ρ. Else if $F' < F_0$, when $F \to 0$, r_d gets infinitely to the imaginary axis. The bandwidth goes to zero. Eventually, r_d lies in between $[0, \rho]$ when F goes from zero to infinity. This implies that wherever the poles are placed, the bandwidth is more likely to reduce to zero due to the variation of F. That is not expected to take place. But it is worth noting that in practice, F value is bounded. Based on the definition of F, the variation range can be verified.

Initially, according to the function definition of *fal*, nonlinear parameter F will be calculated as below:

$$F = \frac{fal(e_1)}{e_1} = \begin{cases} |e_1|^{\alpha-1}, & |e_1| > \delta \\ \delta^{\alpha-1}, & |e_1| \le \delta \end{cases} \tag{22}$$

From (22), it is known that F varies monotonically with respect to e_1 and lies in between $[0, \delta^{\alpha-1}]$. As e_1 goes to infinity, F gets to zero. But this is impractical since only if the observer becomes unstable, there will exist this situation. However, the stability of the closed-loop system can be guaranteed by the controller design. The stability of the observer can be guaranteed by the selection of the parameters. Therefore, for the actual system, it can be assumed that the observer error e_1 is always less than a certain threshold. Therefore, the range of F is $[e_{max,}^{\alpha-1}, \delta^{\alpha-1}]$. In order to minimize the poles in the specified range, the ESO parameter configuration method is considered. The following conditions must be met:

(1) Based on the dynamics of the total disturbance g, set the disturbance observation bandwidth ω_c.
(2) Given the maximum value of the tracking error e_1, determine the high and low points for the nonlinear parameter F according to the characteristics of the fal function and obtain the variation range.
(3) Ensure that the observer bandwidth covers that of the disturbance with respect to the range of F.

From (21), r_2 represents the minimum distance to the imaginary axis which is also the bandwidth of the observer.

$$r_2 = -\rho + \rho/2\cdot\sqrt[3]{1-F'/F_{op}}\left(\sqrt[3]{1+\sqrt{F'/F_{op}}} + \sqrt[3]{1-\sqrt{F'/F_{op}}}\right) \tag{23}$$

To remedy the influence of F, the second term of (23) must be zero such that r_2 reaches its peak value. The following three optimal gains that will produce better performance are given as below.

$$\beta_1 = 3\rho,\ \beta_2 = 3\rho^2/F \text{ and } \beta_3 = \rho^3/F \tag{24}$$

Using the above method, the maximum bandwidth keeps consistent with ρ no matter how F changes after the pole assignment. Also the bandwidth will maintain within the range specified by the two boundary points. It is proved that this method can ensure that ρ covers ω_c, that is, the bandwidth of ESO will not vary with F. From (24), this also means that the observer gains must be set larger. Therefore, the proposed observer parameter configuration method is optimal.

IV. Experimental Results

The sensorless capability of the proposed observer TNESO is experimentally verified. The test rig consists of a dSPACE based AC motor hardware platform, a SEMICUBE inverter and a machine bench as illustrated in Fig. 7. The dSPACE control system includes PPC Processor board (dual-core PowerPC, 2 GHz). The AC Motor Control Solution is based on the DS5202 FPGA Board (14 bit ADC, 12 bit DAC and digital IO). The switching frequency of the SEMICUBE inverter was set to 8kHz. The deadband was 2μs. The basic specifications for the prototype machine are listed in Table 1. Table II gives the observer gains.

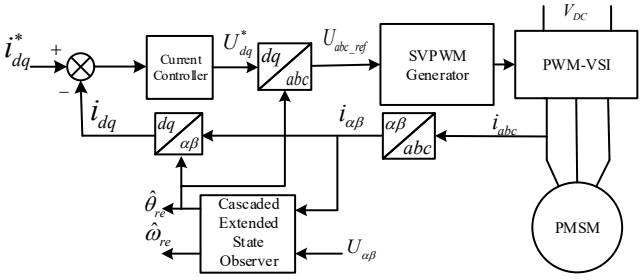

(a)

This article has been accepted for publication in a future issue of this journal, but has not been fully edited. Content may change prior to final publication. Citation information: DOI 10.1109/TPEL.2019.2914119, IEEE Transactions on Power Electronics

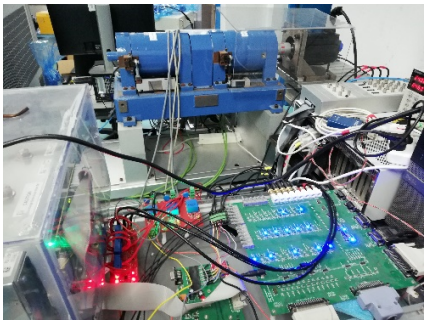

(b)

Fig. 7. Sensorless drive system (a), dSPACE desktop control system, Semikron inverter and its interfacing boards (b).

TABLE I. RATED PARAMETERS OF THE IPMSM USED IN THE EXPERIMENTS

Parameters	Value	Unit
Pole pairs	4	-
Rated speed	1500	Rpm
Rated torque	14.7	N.m
Rated phase current	9.8	A
Rated power	2.3	kW
Rotor pole flux	0.14	V.s
d-axis inductance	2.54	mH
q-axis inductance	4.08	mH
Stator resistance	0.46	Ω

TABLE II. OBSERVER PARAMETERS IN THE EXPERIMENTS

Parameters	Value
β_1	320
β_2	3800
β_3	12500
ρ	100
α	0.5
δ	0.01

The speed feedback loop in sensorless drive system (Fig. 7 (a)) was closed by the estimated speeds to verify the effectiveness of the sensorless control algorithms. The estimated rotor angle is used to do the transformations among the different reference frames. The Q-PLL is only utilized for comparison. The experiments have been carried out in both the steady-state and transient operations in wide speed range.

A. Steady-state Comparison between TNESO and Q-PLL

In comparison with the conventional Q-PLL scheme, the steady state response of TNESO is demonstrated in this scenario. The IPM motor was operated at 300 rpm with full load. Initially, the speed feedback loop was closed by the speed estimated by TNESO. Then the feedback was switched to the speed produced by Q-PLL for comparison.

In Fig. 8, it can be seen that TNESO exhibits much less ripples on the real speed than the Q-PLL when the motor ran at

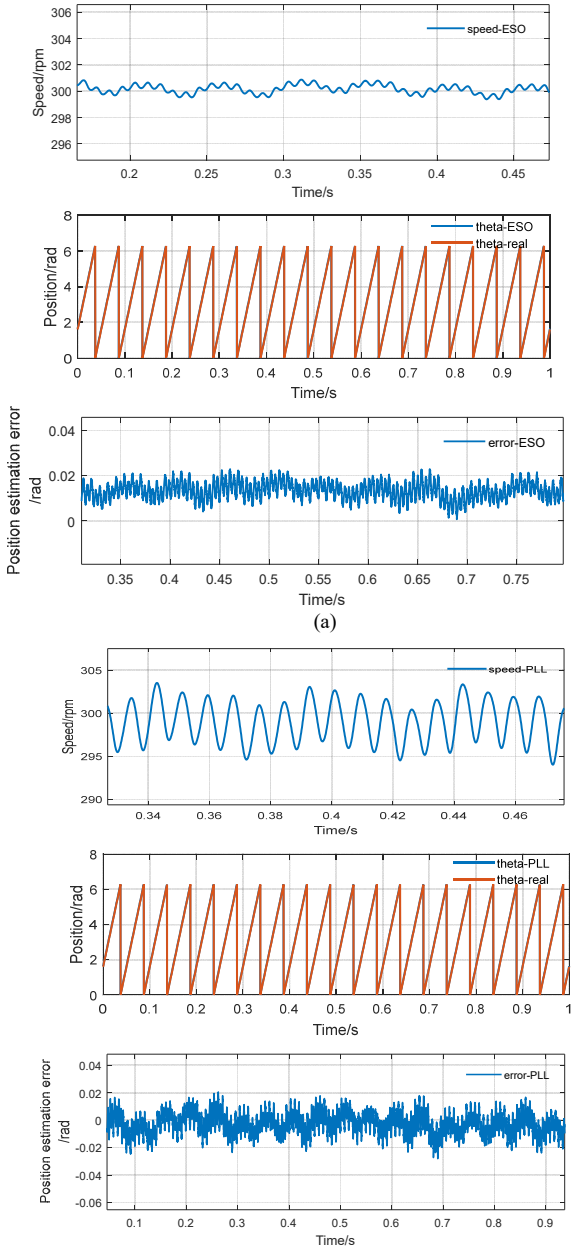

(b)

Fig. 8. Steady-state performance comparison of the proposed TNESO (a) and Q-PLL (b) at 300 rpm with full load. Upper subplots: estimated speed. Middle subplots: actual and estimated positions. Lower subplots: position estimation error.

300 rpm with full load. The maximum ripple of Q-PLL speed reaches 6 rpm while TNESO's real speed is bounded within 1 rpm. The rotor angles estimated by Q-PLL and TNESO are illustrated on the subplots in the middle of Fig. 8. All of them have satisfactory performance. The estimated and actual angles appear to be overlapped. It is still obvious that the estimation error of TNESO is less than 0.023 rad. Apparenly, the estimation error of Q-PLL spans from -0.02 to +0.02 rad. It is concluded that TNESO is able to reduce the error significantly compared to Q-PLL.

This article has been accepted for publication in a future issue of this journal, but has not been fully edited. Content may change prior to final publication. Citation information: DOI 10.1109/TPEL.2019.2914119, IEEE Transactions on Power Electronics

B. Transient Performance in Closed-Loop Sensorless Operations

1) Speed Control Dynamics

This scenario intends to exploit the minimum speeds that both TNESO and Q-PLL control schemes are able to extend downwards the low speed range where the sensorless drive works without any signal injection. The low speed range operations are investigated by feeding back the estimated speed from TNESO and Q-PLL respectively. Firstly, a decreasing speed ramp reference was applied to the speed controller at constant full load. Since the instability threshold is a function of the speed, it is expected that at full torque, there is a minimum speed below which Q-PLL becomes unstable. This is proved by the curve in Fig. 9 (b), which shows an instability arising at 13% the rated speed. Under the same test conditions, the proposed TNESO was stable down to 5.3% of the nominal speed.

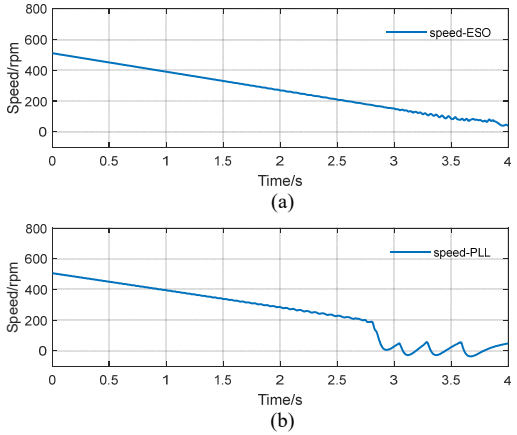

Fig. 9. Slow speed ramp with full load. (a) Proposed TNESO and (b) conventional Q-PLL.

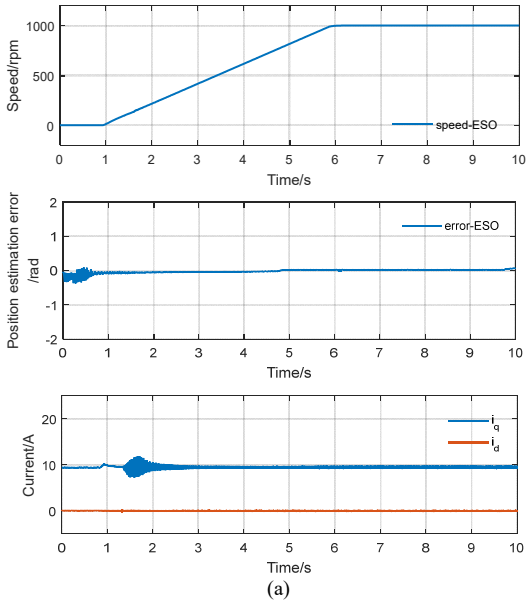

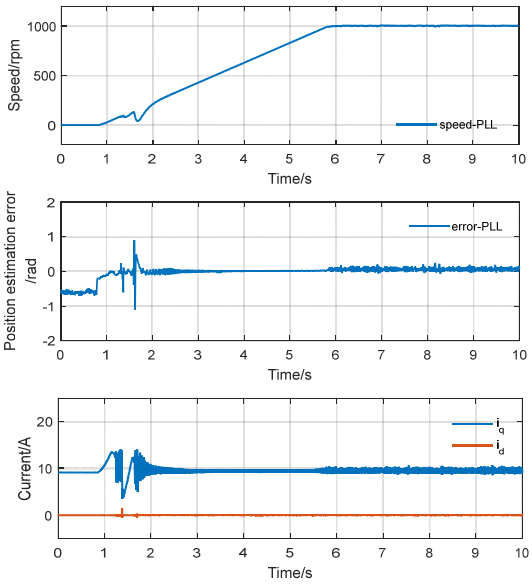

Fig. 10. Closed-loop sensorless control results at start-up with full load. (a) TNESO (b) Q-PLL.

In speed dynamic operations, a comparison of TNESO and Q-PLL was also made and the results are reported in Fig. 10. Since at zero speed, both observers cannot work alone, the IPM motor was started with measured position. At 80rpm, the observers were activated and the feedbacks were commutated to the estimated position and speed. This drawback can be compensated by detecting spatial orientations of the rotor anisotropy below the critical speed. The maximum estimation error of 5 electrical degree occurs at the kick-start. Full loads were applied to test two sensorless control scheme. The proposed TNESO exhibits smooth operations with full load except small torque ripples during the speed transition. The maximum estimated errors appeared at start-off around zero speed where TNESO is not effective. It is found that Q-PLL had difficulty during the speed switching. The torque component i_q experienced aa large turbulence when the feedback switched to the speed produced by Q-PLL. The position estimation by Q-PLL is obvious. During the transients, it almost reaches 1 rad and pushes the system into instability.

2) Load disturbance

Fig. 11 shows the transient speed performance for TNESO with sudden load application and removal of 8N.m. It should be highlighted that the real speed is able to recover in a very short period, which demonstrates the drive's capability of rejecting the load disturbances effectively. The TNESO's estimated angle has much less estimation error and oscillation in both steady-state and transient period. Hence, TNESO has a significant advantage in load disturbance rejection in closed-loop sensorless operations. Comparison could not be made since Q-PLL was unstable at 100 rpm.

3) Speed Reversal

Fig. 12 is a plot of speed reversal between +500 rpm and -500 rpm with 4N.m load for two schemes. The speed reference

This article has been accepted for publication in a future issue of this journal, but has not been fully edited. Content may change prior to final publication. Citation information: DOI 10.1109/TPEL.2019.2914119, IEEE Transactions on Power Electronics

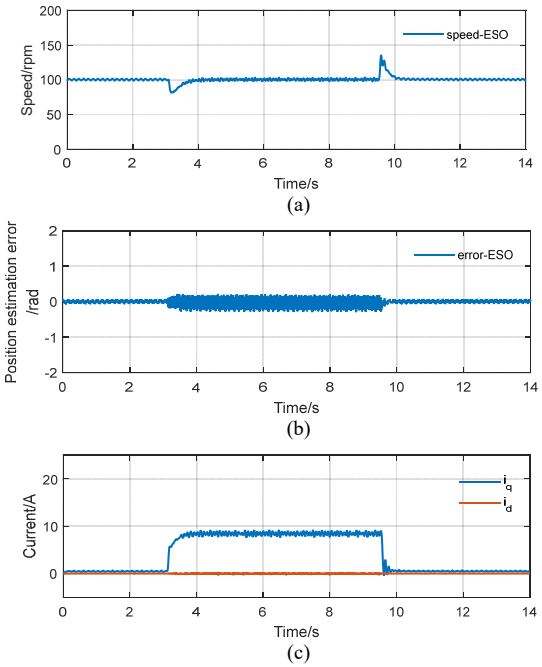

Fig. 11. Transient performance of TNESO with sudden load variations of 8N.m. (a) Real speed of TNESO (b) Position estimation errors (c) The stator currents in *d-q* reference frame.

is a trapezoidal signal with an amplitude of 500 rpm. It is seen that the real speed of TNESO is accurate and the ripples are minimized. The speed response tracked the reference very well. At very low speed, TNESO responded in a very short time and generated very little spike in overcoming the effect of the instability caused by the very low speed and massive load. The potential reluctance torque of the IPMSM had been fully exploited. Maximum Torque Per Ampere (MTPA) control has been adopted to increase the torque production in the constant torque region for the IPMSMs. In Fig. 12 (b), the measured currents tracked MTPA trajectory below the rated speed. The robustness of TNESO and the performance of the drive system on heavy load torque at low and medium speed have been verified by the results.

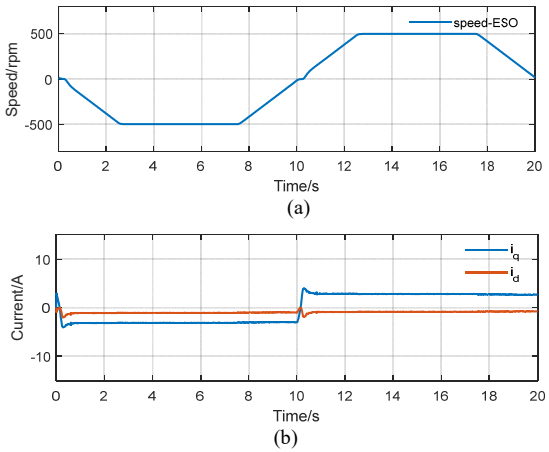

Fig. 12. Speed reversal of TNESO and PLL under MTPA control between +500 rpm and -500 rpm with 4N.m load. (a) Real speed. (b) Stator currents in *d-q* reference frame.

4) *Accurate and Fast Estimation of Total Disturbance*

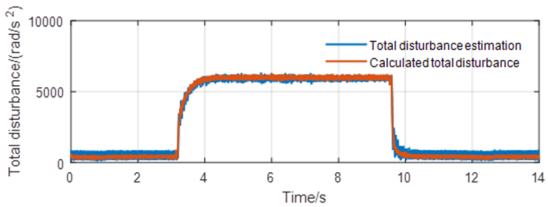

Fig. 13. Illustrations of the estimated disturbance g, under the step load variations under the testing condition of Fig. 11.

In Fig. 13, the estimated total disturbance g is plotted. Under the sudden full load application and removal, the total disturbance is estimated accurately at a fast rate. Correspondingly, the position and speed estimation are compensated. As the value of the observer bandwidth is set sufficiently high, the radius of convergence gets close to zero. To reduce the effects of the uncertainty, the selection of observer bandwidth must be sufficiently extended. The optimal fast tracking observer bandwidth is dependent of F and the inverse of sampling time.

C. *Sensitivity Analysis*

The estimation errors due to the influence of parameter detuning and dynamics mismatch are analyzed experimentally. The perturbations to the parameter Δa, Δb and Δc are strong functions of the moment of inertia J. Therefore, the effect of the variation of J is most influential. The real value of J is varied by $\pm$20% of the nominal value due to the identification error. Experimental tests were carried out at three meaningful load points, i.e., at 0%, 50% and 100% the nominal load. From Fig. 14, it is seen that in high speed region, the TNESO delivers the most accurate speed estimation under no-load condition and without mismatches. At low speed, the maximum error is 7rpm at 100rpm with 20% mismatch. With the load torque increases, the maximum estimation error slightly decreases. At 50% the rated load, the peak error drops to around 5.5 rpm. When full load was applied. 20% detuning of inertia affects the observer performance more than for a 50% the nominal load. The peak error of 5rpm occurs for the case of 20% mismatch at 100rpm at full load.

L_q falls as the operating current increases. The effects caused by L_d and L_q detuning have been investigated in this paper. The experimental tests were carried out when the machine was operated at 500 rpm with various loads up to full load. Fig. 15(a) is a plot of the peak position estimation errors that are subjected to various load changes, nominal L_d and L_q versus 60% nominal L_d and L_q. In Fig. 15 (b), the blue line is the reference without mismatch. To verify the effect of flux changing, only λ_f was varied and the rest was unchanged. The parameter variation was 60% of the nominal values separately. From the comparison, it has been verified that the estimation errors due to L_d, L_q and λ_f increase under light load condition. At no load, the estimation errors reached above 0.01 rad.. As the load goes up towards rated value, the errors slightly changes.

This article has been accepted for publication in a future issue of this journal, but has not been fully edited. Content may change prior to final publication. Citation information: DOI 10.1109/TPEL.2019.2914119, IEEE Transactions on Power Electronics

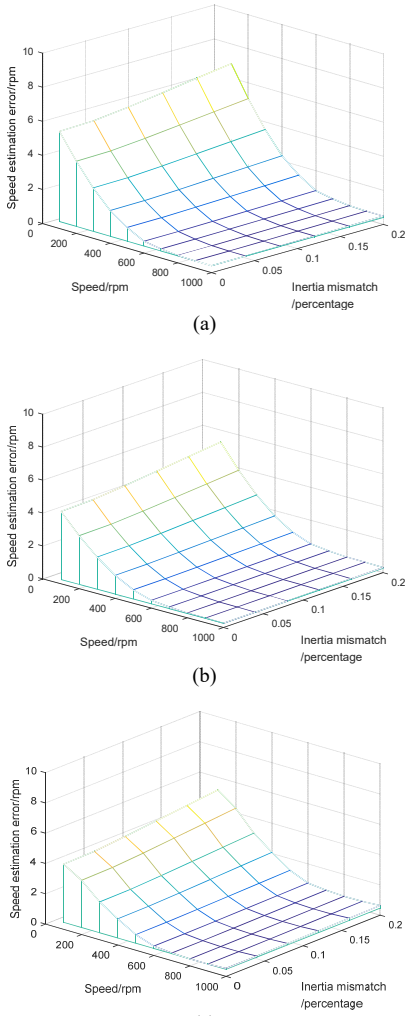

Fig. 14. Speed estimation errors due to J mismatches at 0% nominal load (a), 50% rated load (b) and 100% the nominal load torque (c).

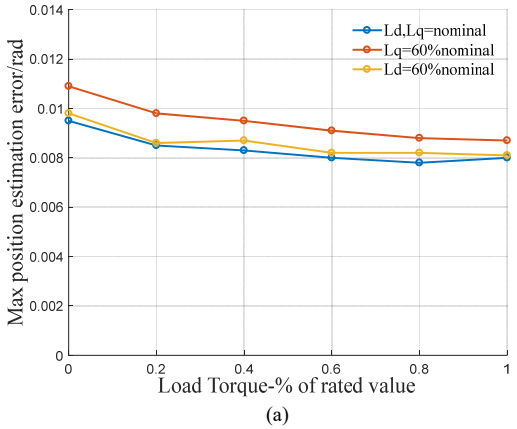

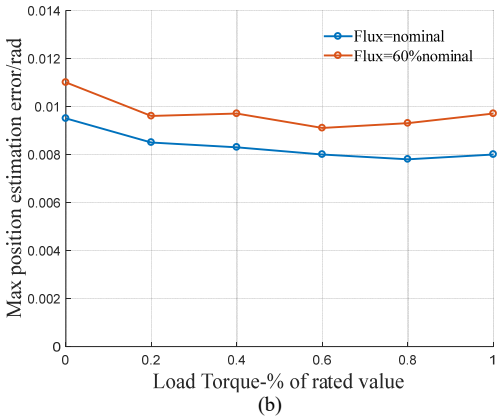

Fig. 15. Maximum speed estimation errors due to mismatches of L_d and L_q (a) and λ_f (b) with various loads up to full load.

CONCLUSION

In this paper, a third order extended state observer has been proposed to estimate the rotor position and speed of IPMSM drives. Stability analysis and a procedure to design the ESO optimal gains have been provided. Extensive experimental results validate the theoretical contributions in comparison with Q-PLL. In the closed–loop sensorless operation, the proposed ESO has enhanced the estimation performance even in the case that the speed reference or the load torque varies rapidly. The estimation errors have been found to be smaller than commonly-used Q-PLL both in steady state and dynamic operations. It has been proven that the proposed sensorless control strategy is more effective for sensorless IPMSM drives.

REFERENCES

[1] F. Mwasilu and J. Jung, "Enhanced Fault-Tolerant Control of Interior PMSMs Based on an Adaptive EKF for EV Traction Applications," in *IEEE Trans. Power Electron.*, vol. 31, no. 8, pp. 5746-5758, Aug. 2016.

[2] D. Reigosa, D. Fernandez, T. Tanimoto, T. Kato and F. Briz, "Comparative Analysis of BEMF and Pulsating High-Frequency Current Injection Methods for PM Temperature Estimation in PMSMs," in *IEEE Trans. Power Electron*, vol. 32, no. 5, pp. 3691-3699, May 2017.

[3] T. Tuovinen, M. Hinkkanen, L. Harnefors, and J. Luomi, "Comparison of a reduced-order observer and a full-order observer for sensorless synchronous motor drives," *IEEE Trans. Ind. Appl.*, vol. 48, no. 6, pp. 1959–1967, Nov. 2012.

[4] R. Bojoi, M. Pastorelli, J. Bottomley, P. Giangrande, and C. Gerada,"Sensorless control of PM motor drives—A technology status review," in Proc. *IEEE Workshop Elect. Mach. Des. Control Diagnosis*, Mar. 2013, pp. 168–182.

[5] L. Rovere, A. Formentini, A. Gaeta, P. Zanchetta and M. Marchesoni, "Sensorless Finite-Control Set Model Predictive Control for IPMSM Drives," in *IEEE Trans. Ind. Electron.*, vol. 63, no. 9, pp. 5921-5931, Sept. 2016.

[6] Y. Kano and N. Matsui, "Sensorless control of interior permanent magnet synchronous motor: An overview and design study," *2017 IEEE Workshop on Electrical Machines Design, Control and Diagnosis* (WEMDCD), Nottingham, 2017, pp. 199-207.

[7] S. Bolognani, L. Tubiana, and M. Zigliotto, "Sensorless control of PM synchronous motors with non-sinusoidal back EMF for home appliance," in *Proc. IEEE IEMDC*, vol. 3. Jun. 2003, pp. 1882–1888.

[8] S. Sul, Y. Kwon and Y. Lee, "Sensorless control of IPMSM for last 10 years and next 5 years," in *CES Transactions on Electrical Machines and Systems*, vol. 1, no. 2, pp. 91-99, 2017.

[9] Orlowska-Kowalska T, Dybkowski M. , "Stator Current Based MRAS Estimator for a Wide Range Speed Sensorless Induction Motor Drive," in *IEEE Trans. Ind. Electron.*, 2010, 57(4): 1296-1308.
[10] L. Sheng, W. Li, Y. Wang, M. Fan and X. Yang, "Sensorless Control of a Shearer Short-Range Cutting Interior Permanent Magnet Synchronous Motor Based on a New Sliding Mode Observer," in *IEEE Access*, vol. 5, pp. 18439-18450, 2017.
[11] Zhou T. , "Expansive State Observer Based on Inverse Hyperbolic Sine Function," *Control and Decision*, 2015, 30 (5): 943-946.
[12] D. Raca, P. Garcia, D. Reigosa, F. Briz, and R. Lorenz, "Carrier-signal selection for sensorless control of PM synchronous machines at zero and very low speeds," *IEEE Trans. Ind. Appl.*, vol. 46, no. 1, pp. 167–178, Jan 2010.
[13] Y. Hua, M. Sumner, G. Asher, Q. Gao and K. Saleh, "Improved sensorless control of a permanent magnet machine using fundamental pulse width modulation excitation," in *IET Electric Power Applications*, vol. 5, no. 4, pp. 359-370, April 2011.
[14] N. Bianchi, S. Bolognani, J. H. Jang, and S. K. Sul, "Comparison of PM motor structures and sensorless control techniques for zero-speed rotor position detection," *IEEE Trans. Power Electron.*, vol. 22, no. 6, pp. 2466–2475, Nov. 2007.
[15] G. Wang, Z. Li, G. Zhang, Y. Yu and D. Xu, "Quadrature PLL-Based High-Order Sliding-Mode Observer for IPMSM Sensorless Control With Online MTPA Control Strategy," in *IEEE Transactions on Energy Conversion*, vol. 28, no. 1, pp. 214-224, March 2013.
[16] G. Zhang, G. Wang, D. Xu and N. Zhao, "ADALINE-Network-Based PLL for Position Sensorless Interior Permanent Magnet Synchronous Motor Drives," in *IEEE Trans. Power Electron.*, vol. 31, no. 2, pp. 1450-1460, Feb. 2016.
[17] J. Han, "From PID to Active Disturbance Rejection Control," *IEEE Trans. Ind. Electron*, vol. 56, pp. 900-906, 2009.
[18] Z. Gao, ''Scaling and bandwidth-parameterization based controller tuning'', in *Proc. of the 2003 American Control Conference*, Denver, CO, USA. June 2003, pp. 4989–4996.
[19] J. Li, Y. Xia, X. Qi and Z. Gao, "On the Necessity, Scheme, and Basis of the Linear–Nonlinear Switching in Active Disturbance Rejection Control," in *IEEE Trans. Ind. Electron*, vol. 64, no. 2, pp. 1425-1435, Feb. 2017.
[20] W. Xue, R. Madonski, K. Lakomy, Z. Gao and Y. Huang, "Add-On Module of Active Disturbance Rejection for Set-Point Tracking of Motion Control Systems," in *IEEE Trans. Ind. Appl.*, vol. 53, no. 4, pp. 4028-4040, July-Aug. 2017.
[21] Zhiqiang Gao, "On the centrality of disturbance rejection in automatic control," ISA Transactions, Volume 53, Issue 4, 2014, Pages 850-857.
[22] Madonski, R., "Herman, P. Survey on methods of increasing the efficiency of extended state disturbance observers,". *ISA Trans.* 2015, 56, 18–27.
[23] G. Wang, H. Zhan, G. Zhang, X. Gui and D. Xu, "Adaptive Compensation Method of Position Estimation Harmonic Error for EMF-Based Observer in Sensorless IPMSM Drives," in *IEEE Trans. Power Electron.*, vol. 29, no. 6, pp. 3055-3064, June 2014.
[24] G. Wang, T. Li, G. Zhang, X. Gui and D. Xu, "Position Estimation Error Reduction Using Recursive-Least-Square Adaptive Filter for Model-Based Sensorless Interior Permanent-Magnet Synchronous Motor Drives," in *IEEE Trans. Ind. Electron*, vol. 61, no. 9, pp. 5115-5125, Sept. 2014.
[25] Z. Tang, X. Li, S. Dusmez and B. Akin, "A New V/f-Based Sensorless MTPA Control for IPMSM Drives," in *IEEE Trans. Power Electron.*, vol. 31, no. 6, pp. 4400-4415, June 2016.
[26] Y.-D. Yoon, S.-K. Sul, S. Morimoto, and K. Ide, "High-bandwidth sensorless algorithm for AC machines based on square-wave-type voltage injection," *IEEE Trans. Ind. Appl.*, vol. 47, no. 3, pp. 1361–1370, May/Jun. 2011.
[27] Y. Lee and S. Sul, "Model-Based Sensorless Control of an IPMSM With Enhanced Robustness Against Load Disturbances Based on Position and Speed Estimator Using a Speed Error," in *IEEE Trans. Ind. Appl.*, vol. 54, no. 2, pp. 1448-1459, March-April 2018.